NRIAG JOURNAL OF ASTRONOMY AND GEOPHYSICS
2019, VOL. 8, NO. 1, 22–33
https://doi.org/10.1080/20909977.2019.1615795



# Tectonic and structural analysis of the Migmatite–Gneiss–Quartzite complex of Ilorin area from aeromagnetic data

O. B. Balogun

Department of Geology, Obafemi Awolowo University, Ile-Ife, Nigeria

**ABSTRACT**

In an effort to have better understanding of the geologic settings and structural disposition of the Nigerian basement rocks, Ilorin area, a notably complex region within the South-western Basement Complex of Nigeria was studied using aeromagnetic data so that existing knowledge on the geology of the area can be appraised and updated. The aeromagnetic data was enhanced using various techniques which include the Total Horizontal Derivative (THD), Standard Euler Deconvolution, Tilt Derivative and Spectral Analysis. Striking features observed over the Residual Magnetic Field map were NE-SW trending anomalies aligned diagonally and running from the SW to the NE, forming a band having a width of between 16,000 and 20,000 m that coincided with the Banded Gneiss region on the geologic map; conspicuous E-W trending magnetic low whose location lies very close to the boundary between Migmatite and Banded Gneiss; and a ring-like magnetic low occurring in the south-eastern part of the residual map with no surface expression on the geologic map. Residual Magnetic Field values ranged from +157 to −202 nT. The THD map showed that the Banded Gneiss was the most deformed unit within the Migmatite–Gneiss–Quartzite complex. Major fractures coincident with Banded Gneiss boundaries appeared to be possible channels from which heat was leached in the regional system during metamorphism such that the Banded Gneiss region attained a relatively lower grade metamorphism than the Migmatite sharing boundary with it. Result from the spectral analysis showed that the magnetic basement in the eastern region was downthrown abruptly relative to that in the western portion. The abruptness was interpreted to mean that such subsidence was fault controlled. The study concluded that the presence of major fractures interfering with metamorphic processes in a regional settings may influence the grades of metamorphism that may result; that the schist region in the study area could be overlying a region of downthrown bedrock; and that the stress pattern that defined the crustal deformation pattern at the near crust in the past had changed compared to the currently dominant pattern.

**KEYWORDS**

South-western Basement Complex of Nigeria; Migmatite–Gneiss–Quartzite complex; Schist Belt; residual magnetic field; magnetic basement; structural disposition

## 1. Introduction

From the series of studies conducted on the "Nigerian Proterozoic crustal development during the Pan-African Regime" between the 1960s and the early 1990s, three broad lithologies have been identified. These are the polymetamorphic Migmatite–Gneiss complex which is composed largely of migmatites and gneisses of various compositions and amphibolites; low-grade sediments-dominated Schists which form narrow belts to the west of longitude 8° E; and the syntectonic to late tectonic granitic rocks which cut both the Migmatite–Gneiss complex and the Schist Belts (Turner 1983; Ajibade et al. 1987). These basic lithologies have been found to be distinguished within the Nigerian Basement Complex (Figure 1).

But during the years that followed this period of extensive regional studies on the development and evolution of the Nigerian basement rocks, except for a few works which were purely geochronology studies (Dada 1998, 1999), lesser scaled studies designed towards more detailed understanding of the peculiar geologic settings across distinguished geologic regions were not conducted to appraise existing discoveries and the implication of this has been that no new, significant insight was gained about the geologic settings and structural disposition of the Nigerian basement rocks.

In an effort to have better understanding of the geologic settings and structural disposition of the Nigerian basement rocks, Ilorin area, a notably complex region within the South-western Basement Complex of Nigeria was studied on a less regional (semi-regional) scale using magnetic (aeromagnetic) data so that existing knowledge on the geology of the area can be appraised and updated

Ilorin area is a region of complex geology. Within the region, there is a notable occurrence of an extensive Migmatite–Gneiss–Quartzite complex and Schist Belt (Egbe-Isanlu Schist Belt) adjacent to each other. The schist is also believed to be intruded by granitic bodies.

Nigerian schists are generally localised to the western part of country and none existed outside longitude 8° E. A lot is yet to be understood about their process of

**CONTACT** O. B. Balogun balogun.timilehin2015@gmail.com Obafemi Awolowo University, Ile-Ife, Nigeria

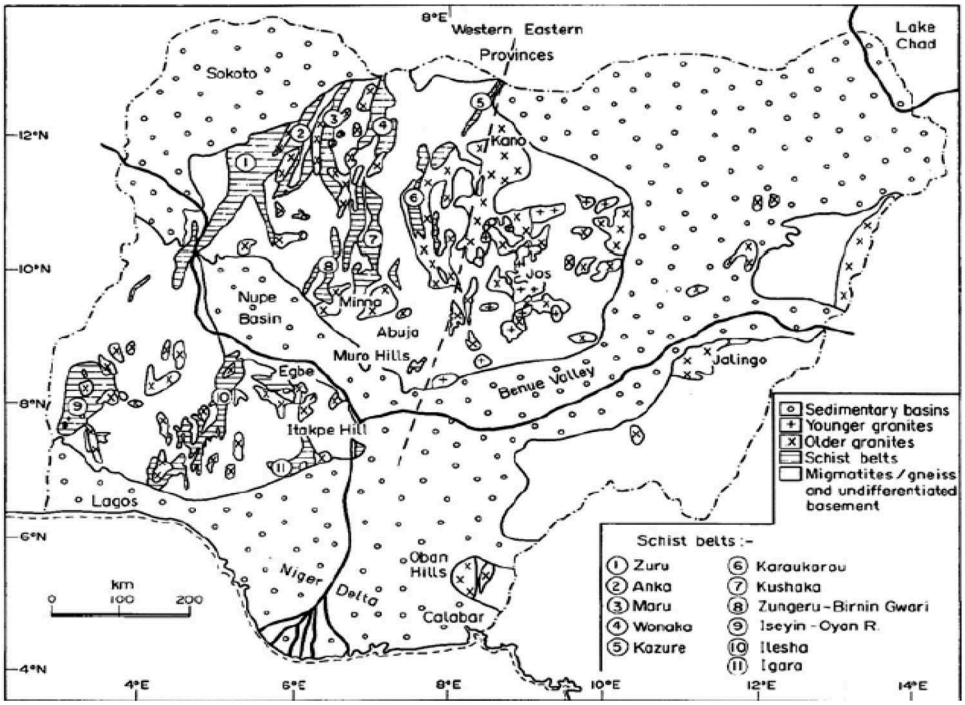


**Figure 1.** The geological map of Nigeria showing the Schist Belts (after Woakes et al. (1987)).

structural and evolution with the most popular proposition about its evolution being that they (schists of the younger metasediments) are relics of a supracrustal cover, which was probably infolded into narrow N-S trending synformal furrows (Turner 1983; Ajibade et al. 1987). This study was designed to derive as many as possible structural and geologic information about Ilorin area from the analysis of the high-resolution aeromagnetic data acquired over the area.

## 2. The study area

The study was carried out around Ilorin and environs, southern Kwara State, Nigeria. The study area spans between longitude 4.50–5.00° E and latitude 8.00–8.50° N. Expressed in Universal Traverse Mercator (UTM) coordinates, it is located between 884,000–940,000 m N and 665,000–720,500 m E within Zone 31N of Minna Datum. The land area covered is 55 km × 55 km. Elevation in the study area ranged between 162 and 659 m (Figure 2). The elevation is highest at the south-eastern region and lowest at the northern region. The vegetation is a typical rainforest vegetation characterised by scattered trees and grasses. Some towns within the study area include Ilorin, Igbaja, Oro, Ajese-Ipo, Offa and Erin-Ile.

## 3. The geologic settings of the study area

The study area falls within the South-western Nigerian Basement Complex. It is underlain by the Migmatite–Gneiss–Quartzite complex of Precambrian to Cambrian age intruded by suites of granitic bodies (porphyritic granite, medium/coarse-grained biotite granite, hornblende granite, granodiorite and granite gneiss) known as the Older Granitoids, which are of Pan-African age in the northern, central and south-western regions. Younger metasedimentary rocks, probably of Pan-African age, underlie the south-eastern part of the study area (Figure 3).

Migmatite–Gneiss–Quartzite complex rocks constitute about 75% of the rocks occurring in the area and include Migmatite Gneiss, Banded Gneiss, Granite Gneiss and Quartzite. The Younger Metasediment rocks in the area include the schist and flaggy quartzite, which constitute about 20% of the rocks found in the study area (Figure 3). While the Younger Metasediments, as shown on the geologic map (Figure 3), only occurred at the south-eastern region, the Migmatite–Gneiss–Quartzite complex rocks continued to the east of the study area to areas like Ajegunle, Oko-Baba, Illofa, Eruku, etc. (in Kwara State, Nigeria), which were not covered by the study area. This means that on a more regional scale, the Younger Metasediments occur as lithological entities within the Migmatite–Gneiss–Quartzite complex rocks (Figure 1).

## 4. Materials and methods

### 4.1. Data description

#### 4.1.1. The elevation data

The elevation data used for the study is the high-resolution, Shuttle Radar Topographic Mission (SRTM) global elevation data (Digital Terrain Elevation Data – DTED®) having a spatial resolution of 30 m × 30 m (1 arc second) and a near world-wide coverage. The data was acquired

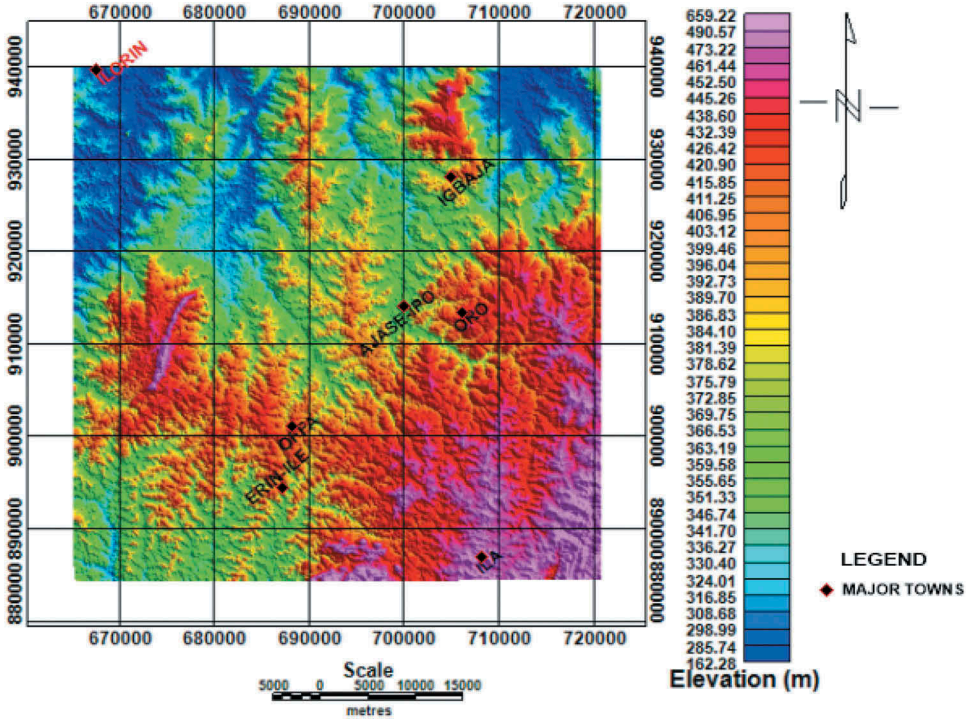


**Figure 2.** The Digital Terrain Elevation Data (obtained from SRTM (USGS 2006)).

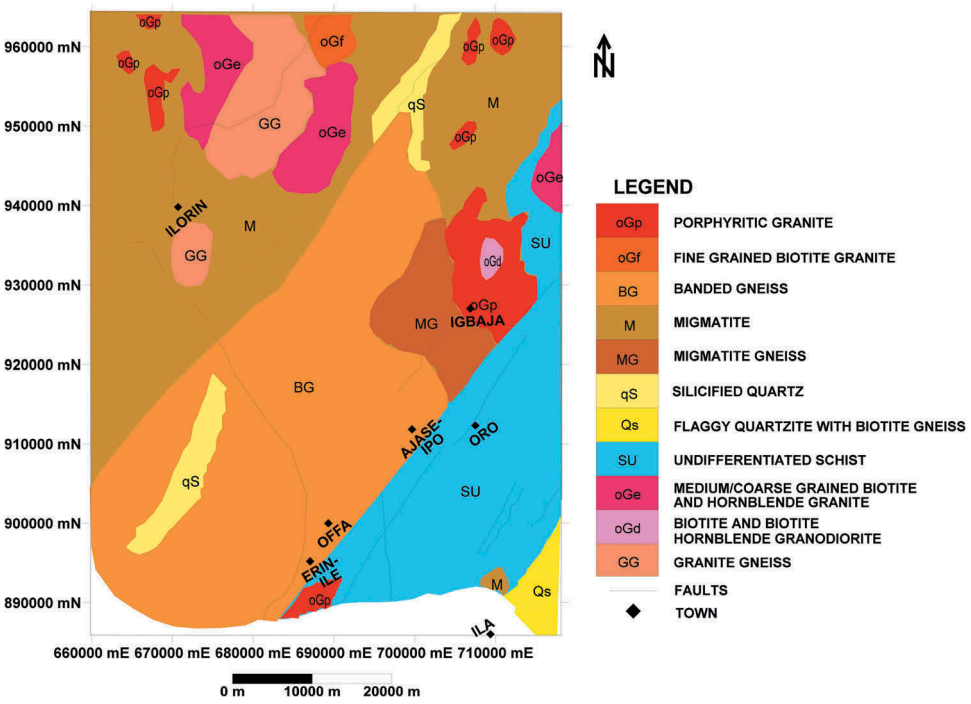


**Figure 3.** The geologic map of the study area. Digitised after Nigerian Geological Survey Agency, 2006.

by radar interferometry and made use of the Earth's Gravity Model 1996 vertical datum. The unit of height measurement is metre (m) and the C-band wavelength is 5.6 cm.

### 4.2. The aeromagnetic data

The magnetic data used for the study is the high-resolution 100 m × 100 m grid aeromagnetic (Total Magnetic Field Intensity (TMI)) data, having a mean terrain clearance of 80 m and recording interval of 0.1 s, acquired by the Nigerian Geological Survey Agency between 2003 and 2010. For this study, the data was reduced to the magnetic equator to remove asymmetries associated with low magnetic latitude anomalies. The regional field was removed and the resulting residual field was processed and analysed.

### 4.3. Aeromagnetic data analysis

The first-order residual field anomaly was obtained by removing the effect of the deep-seated sources (regional field) from the Total Magnetic Field Intensity (TMI) data and enhanced using various techniques. The enhancement was imperative so that subtle magnetic signatures, especially those related to edge detection, can be revealed. The suite of signal enhancement techniques employed includes the Total Horizontal Derivative (THD), Standard Euler Deconvolution, Tilt Derivative (TDR) and Spectral Analysis. The THD and the Standard Euler Deconvolution were basically employed to analyse structures (from the magnetic data), while TDR and Spectral Analysis were employed to evaluate the depth to the magnetic basement.

### 4.4. Total Horizontal Derivative (THD)

The THD technique is the simplest approach to estimate contact locations of bodies at depths (Ndougsa-Mbarga et al. 2012; Oyeniyi et al. 2016). According to Phillips (2000), the horizontal derivative method will produce apparent contacts that are linear and very continuous. The biggest advantage of this method is its low sensitivity to noise in the data because it only requires calculations of the two first-order horizontal derivatives of the field (Phillips 2002). Hogg (2004) describes horizontal derivatives as being essentially important, while trying to map linear features such as fault zones and/or dykes from potential field data. If $T$ is the magnetic field, then the THD is given by:

$$\mathrm{THD}(\mathrm{x},\mathrm{y}) = \sqrt{\left(\frac{\partial \mathrm{T}}{\partial \mathrm{x}}\right)^2 + \left(\frac{\partial \mathrm{T}}{\partial \mathrm{y}}\right)^2} \qquad (1)$$

where $x$ and $y$ are the directions of differentiation

Maxima observed on THD map are diagnostic of lineaments (faults and lithologic contacts) and their locations within the study area. In order to highlight the contacts shown on the THD map, the maxima of the THD map were plotted as thick black lines on the THD map where the peaks are continuous.

### 4.5. 3-D standard Euler deconvolution

This technique provides estimates of source location and depth. Therefore, Euler Deconvolution is both a boundary finder and depth estimation technique. Euler Deconvolution is commonly employed in potential field data interpretation because it requires only a little prior knowledge about the source geometry, and more importantly, it requires no information about the magnetisation vector in the case of magnetics (Thompson 1982; Reid et al. 1990; Balogun et al. 2016; Oyeniyi et al. 2016) such that its solutions are not affected by assumptions about presence or absence of remanence. The technique determines the anomaly position, depth and base level for a specific magnetic source across a study site. The standard 3-D Euler Deconvolution is based on solving Euler's homogeneity equation (Equation 2) (Reid et al. 1990):

$$(\mathrm{x} - \mathrm{x}_0)\frac{\partial \mathrm{T}}{\partial \mathrm{x}} + (\mathrm{y} - \mathrm{y}_0)\frac{\partial \mathrm{T}}{\partial \mathrm{y}} + (\mathrm{z} - \mathrm{z}_0)\frac{\partial \mathrm{T}}{\partial \mathrm{z}} = \eta(\beta - \mathrm{T}) \qquad (2)$$

which can be re-written as:

$$\mathrm{x}\frac{\partial \mathrm{T}}{\partial \mathrm{x}} + \mathrm{y}\frac{\partial \mathrm{T}}{\partial \mathrm{y}} + \mathrm{z}\frac{\partial \mathrm{T}}{\partial \mathrm{z}} + \eta \mathrm{T} = \mathrm{x}_0\frac{\partial \mathrm{T}}{\partial \mathrm{x}} + \mathrm{y}_0\frac{\partial \mathrm{T}}{\partial \mathrm{y}} + \mathrm{z}_0\frac{\partial \mathrm{T}}{\partial \mathrm{z}} + \eta\beta \qquad (3)$$

where $\beta$ is the regional value of the potential field and $(x_0, y_0, z_0)$ is the position of the source, which produces the total potential field $T$ measured at $(x, y, z)$. $\eta$ is the called structural index.

### 4.6. Tilt derivative

The Tilt Derivative is obtained from the arc tangent of the ratio of the first vertical derivative to the total horizontal derivative. It differs from the local phase in that it uses the value of the total horizontal derivative in the denominator instead of the derivative in the $x$ direction used in local phase angle determination. The TDR is given as:

$$TDR = tan^{-1}\left[\frac{VDR}{THD}\right] \qquad (4)$$

where VDR and THD are the first vertical derivative and total horizontal derivatives of the TMI respectively.

Qualitative analysis of TDR maps has always shown that relatively shallow targets in a region are usually characterised by closely spaced TDR contours, while deeper targets are usually characterised by widely spaced contours over the −45° to +45° band (Salem et al. 2007). Because all amplitudes are restricted to values between $+\pi/2$ and $-\pi/2$ due to the nature of arc tan trigonometric function, the TDR can function as an automatic gain control filter and equalise the amplitude output of TMI anomalies across a grid or along a profile (Verduzco et al. 2004). It should also be noted that the output amplitude of TDR is more dependent on the depth of burial than magnetic susceptibility contrasts.

Over the edges of an anomaly TDR produces zero crossing over edges at geomagnetic inclination of 0° and 90°. Therefore, TDR is better applied for data that have been reduced to the magnetic equator or the magnetic pole.

### 4.7. Spectral analysis

The spectral analysis technique is a technique capable of decomposing signals into their constituent wavenumber compositions. In magnetic surveys, the total magnetic field measured is the integration (continuous sum) of magnetic signals from the ground surface down to the curie depth which can be decomposed into constituent wavenumber (depth) components by the appropriate mathematical functions. Spector and Grants (1970) stated that the depth factor invariably dominates the shape of radially averaged power spectrum of magnetic data. Radially averaged power spectrum implies that the powers for equal length of the wave vector are averaged. The radially averaged power spectrum of a field in a two-dimensional observation plane decreases with increasing depth to the source ($t$) by a factor $e^{-2tr}$, where r is the wave number.

Hence, if the shape of the power spectrum is dominated by the depth factor, the logarithm of the power spectrum should be proportional to $-2tr$, and the depth to the source can be derived directly from the slope of the log radially averaged power spectrum. Connard et al. (1983) stated that since the log radially averaged power spectrum is usually curved, a single power spectrum for a profile or grid may yield up to five depth values (represented on a segmented curve), which seems to indicate the existence of various vertical magnetic interphases in the crust, with the higher wavenumber regions representing shallower depths and the lower wavenumber regions representing deeper depths. Depth values can therefore be obtained by first approximating the log power spectrum as series of segmented straight line and subsequently calculating the slope of individual straight line segment and dividing it by $4\pi$ to yield the corresponding depths for a grid data and dividing it (the slope) by $2\pi$ for a line profile (Naidu 1972).

## 5. Results and discussion

### 5.1. The residual magnetic anomaly map

The residual magnetic anomaly map is shown in Figure 4. The residual map is dominated by elongated anomaly patterns (magnetic highs and lows) with most of them trending in the NE-SW direction and a few in the E-W direction. An interesting thing to note is that the NE-SW trending anomalies are aligned diagonally in a continuous manner, running all the way from the SW to the NE, and have distinctive margins, forming a diagonal band having a width of about 16,000 m at its south-western end and about 20,000 m at its north-eastern end (Figure 4).

The diagonal band region contains both magnetic highs and lows. Most of the E-W trending anomalies found on the map occur outside the diagonal band. Most anomalies found in the north-western end of the map are roughly spherical except for an elongated, conspicuous E-W trending magnetic low (labelled "P") which seemed to break the continuity of the western diagonal band margin, displacing the northern segment of the band margin more to the west. On comparison with the geologic map (Figure 3), the location of the said anomaly "P" (whose centre is

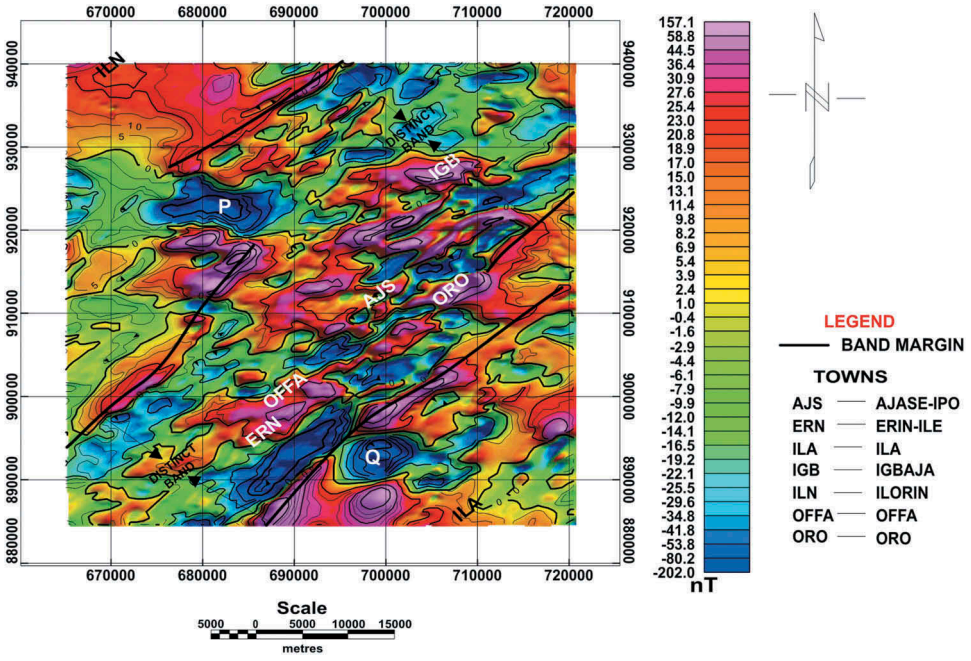


Figure 4. Residual magnetic anomaly map of the study area.

around 680,732 m E, 923,668 m N) lies very close to the boundary between Migmatite and Banded Gneiss.

Another striking anomaly is a ring-like (circular) magnetic low, labelled "Q", occurring in the south-eastern part of the residual map. Having its centre at 699,039 m E and 892,747 m N, it is located just outside the eastern diagonal band margin (Figure 4). From the geologic map (Figure 3), the ring-like anomaly was found to be located within the schist unit and does not have any surface expression.

Due to the fact that the magnetic data were acquired at the magnetic low latitude and were reduced to the equator, magnetic lows (i.e. negative residual field values) indicate high magnetic susceptibility while the magnetic highs (i.e. positive residual field values) indicate low magnetic susceptibility values. Residual Magnetic Field values ranged from +157 to −202 nT.

### 5.2. The total horizontal derivative (THD) map

The THD map of the study area is shown in Figure 5. Since the derivative (in the first order) of a quantity is always maximum where there is an abrupt change (or discontinuity) in the value of that quantity, elongated peak amplitudes on the THD map were taken to indicate positions of structural discontinuity, hence linear geologic features.

The outlined linear features on the map are of two categories. The first category is the relatively short, peak amplitudes outlined with short black lines on the map. These are short linear and curvilinear features having orientation ranging from NE-SW, ENE-WSW to E-W. They occur mostly within the Banded Gneiss region (denoted as "B" on the THD map) and appear to be preferentially concentrated around the lithologic boundaries $M_1$ and $M_2$ which are the boundary between the Banded Gneiss and the Migmatite and the boundary between the Banded Gneiss and the Schist respectively (Figures 3 and 5). This suggests relatively high level of stress, resulting in intense deformation (shearing and foliation) within the Banded Gneiss, especially around its boundaries with adjacent lithologies.

The second category is the relatively longer, continuous, lineaments which are of regional scale outlined (in white lines) and designated as major lineaments (or contacts) on the map. These second category lineaments trend mostly in the NE-SW direction and seem to represent major lithologic boundaries and major fracture lines. While $M_1$ and $M_2$ obviously represent lithological boundaries when compared with the geologic map (Figures 3 and 5), the concentration of many minor lineaments around these lithological boundaries (i.e. $M_1$ and $M_2$) suggests that the lithological boundaries ($M_1$ and $M_2$) themselves might be coincident with fracture zones such that the lithological boundaries were established over some major fractures (joints or faults) trending in the same manner as $M_1$ and $M_2$. This could then explain why we have an extensive body of Banded Gneiss adjacent to an also extensive Migmatite body. Major fractures coincident with boundaries $M_1$ and $M_2$ were possible channels from which heat was removed (leached) in the regional system during metamorphism such that the Banded Gneiss region (bounded by $M_1$ and $M_2$) attained a relatively lower grade metamorphism than the Migmatite adjacent to it.

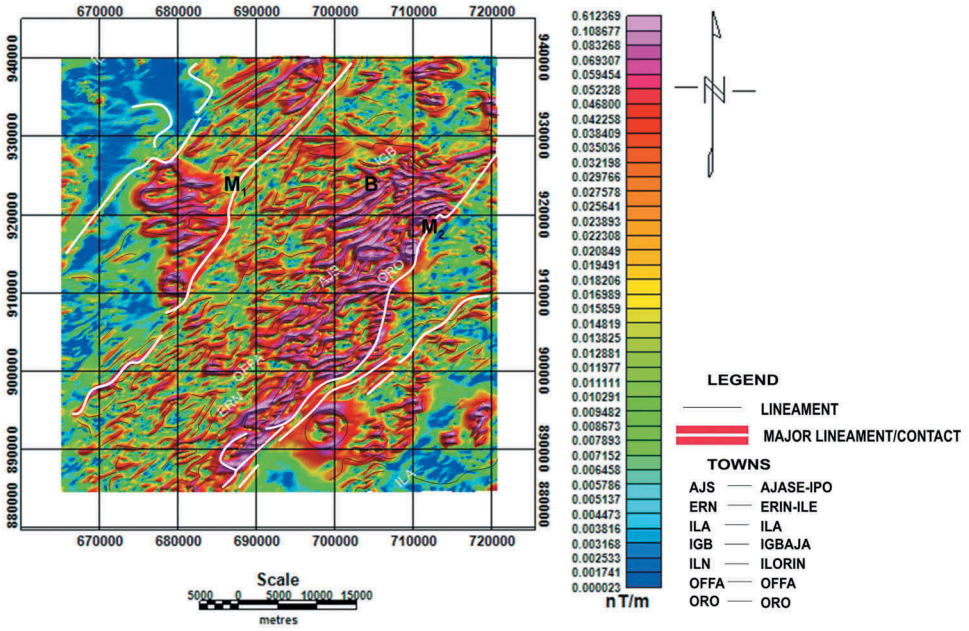


Figure 5. The Total Horizontal Derivative map of the study area.

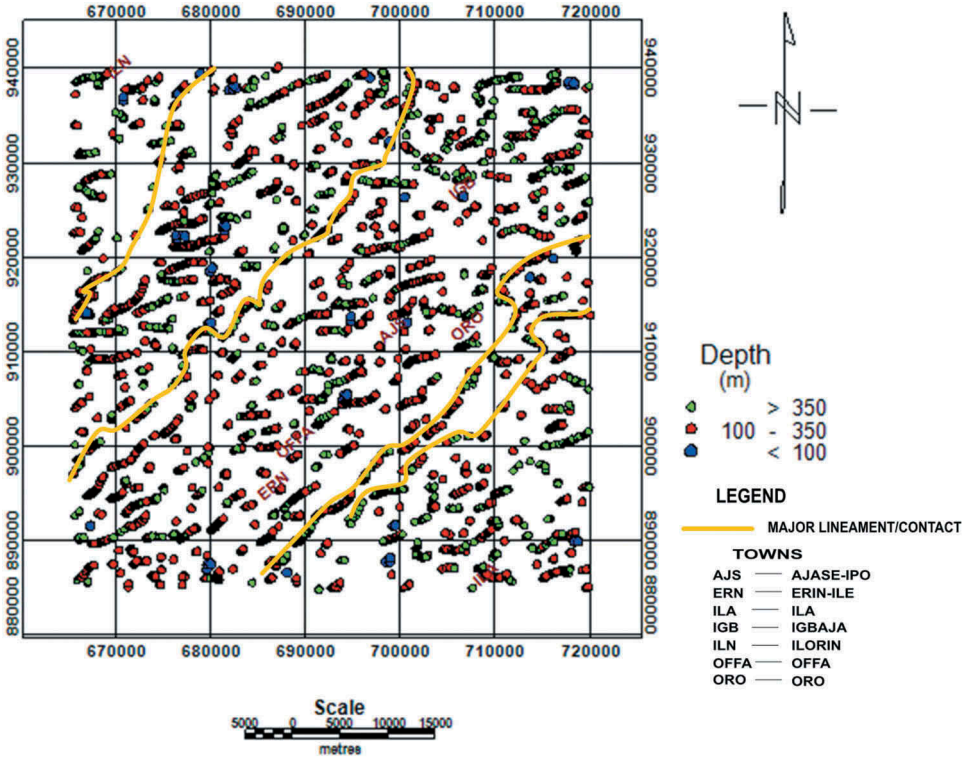


**Figure 6.** Colour-range symbol map plotted for the Euler Deconvolution analysis of the study area.

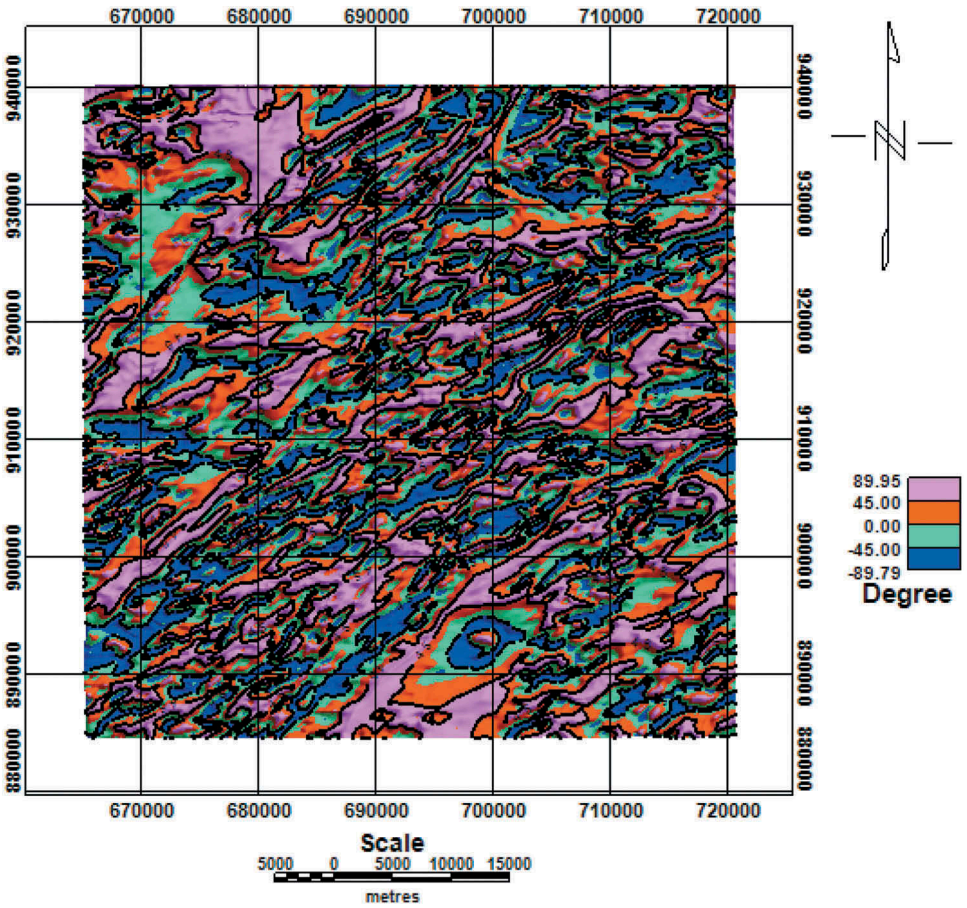


**Figure 7.** Skewed colour-range symbol map of the tilt derivative of the reduced to the magnetic equator field study area. The orange to pale turquoise blue regions depict regions with tilt derivative angle ranging from −45° to 45°.

### 5.3. 3-D standard Euler deconvolution

The plot of the 3-D Standard Euler Deconvolution analysis for the study area was presented in Figure 6 as "colour-range symbol map". The 3-D Standard Euler Deconvolution analysis was used as an alternative means of structural evaluation so that in addition to revealing the orientation of the geologic structures, the continuity of the structures at depth can also be evaluated. However, the Euler solutions accepted were limited to a relatively shallow sub-surface depth (700 m) since the window size that gave the best Euler Deconvolution result was 350 and as such, the maximum depth that can be accepted is 700 m (i.e. twice the window size). The lineaments delineated and the structural trends obtained were well defined and highly comparable with those realised from the THD map. It was however noticeable that the Euler solutions were better defined (i.e. less congested and smoother) than the THD solutions and the structures continued beyond 350 m (Figure 6).

### 5.4. The tilt derivative (TDR)

The TDR map is shown in Figure 7. In the qualitative interpretation of TDR maps, closely spaced contours of the −45° to +45° band usually depict relatively shallow targets while widely spaced contours of the said band do depict relatively deeper targets. Zero degree tilt angles are also believed to form close to edges of bodies, therefore defining source edges, contacts or regions of discontinuities which can all be classified as geologic lineaments in Reduced to the Equator (RTE) data. In the study area, the 0° contour lines follow the same trends and show similar patterns to the lineament patterns delineated on the THD map. In addition, the TDR map suggests that the north-western and south-eastern regions are relatively deeper given that the −45° to +45° band is relatively broader in those regions.

### 5.5. The spectral analysis

In the spectral decomposition of magnetic signals, the depth to the "magnetic basement" is usually taken to be the depth to the "fresh basement rock" either in the basement or sedimentary terrain as the overlying regolith or sediments as the case may be are believed to have negligible magnetic susceptibility in most cases.

Under ideal situation, one would expect that estimated depth to the "magnetic basement" should agree with the depth at which one would encounter the "fresh basement" if someone were to drill into the ground. However, it should be noted that in some cases, the depth to the magnetic basement may appear overestimated with respect to the perceived depth of the fresh basement. This could be due to the fact that the magnetic basement is usually delineated based on the detection of region (depth) where the magnetic susceptibility is found to contrast markedly. And as such, in a situation where in the upper region of the fresh basement there was no marked difference in magnetic susceptibility from the overlying overburden, the depth to the basement rock will most likely be overestimated.

The study area was divided into 16 overlapping square sub-grids with each sub-grid being of 22 km length (Figure 8). Figure 9 shows some of the radially averaged power spectrum plots from the demarcated blocks of the study area used to deduce the depth to the magnetic basement for each of the constituent sub-grid. The depth obtained for each sub-grid was then plotted against a reference coordinate which is the coordinate of the centre of the sub-grid to generate the map of the depth to the top of the basement rock (Figure 10(a,b)).

It was observed that at the western two-third portion of the study area, the depth to the magnetic basement ranged between 0.428 and 0.471 km while at the eastern one-third portion, the depth to the magnetic basement was deduced (from spectral analysis) to be deeper, ranging between 0.477 and 0.602 km (Figure 10(a,b)). The abruptness in the depth change as we move towards the eastern one-third portion of the study area where schist is the principal lithology suggests that the magnetic basement in the region (eastern one-third portion) could have been downthrown relative to that in the western two-third portion. While this inference may not be unique, it is however more plausible to think of the downthrown magnetic basement towards the eastern part as an indication of block subsidence. The abruptness in the displacement would then be an indication that the subsidence was fault controlled.

The coincidental occurrence of the schist within the region of downthrown magnetic basement may however be corroborative of the proposition of geologists who had earlier worked on the crustal development of Nigeria during the Pan-African regime (e.g. Turner 1983; Ajibade et al. 1987) that the schists of the younger metasediments are relics of a supracrustal cover, which was infolded into narrow N-S trending synformal troughs within the fairly stable Migmatite–Gneiss complex.

Profiles taken on Figure 10(a) were stacked and presented as Figure 11. The displacement of the magnetic basement in the eastern region relative to the western regions was vividly pictured. The maximum vertical displacement of the downthrown block (of the eastern region) from the hanging block (of the western region) is 174 m.

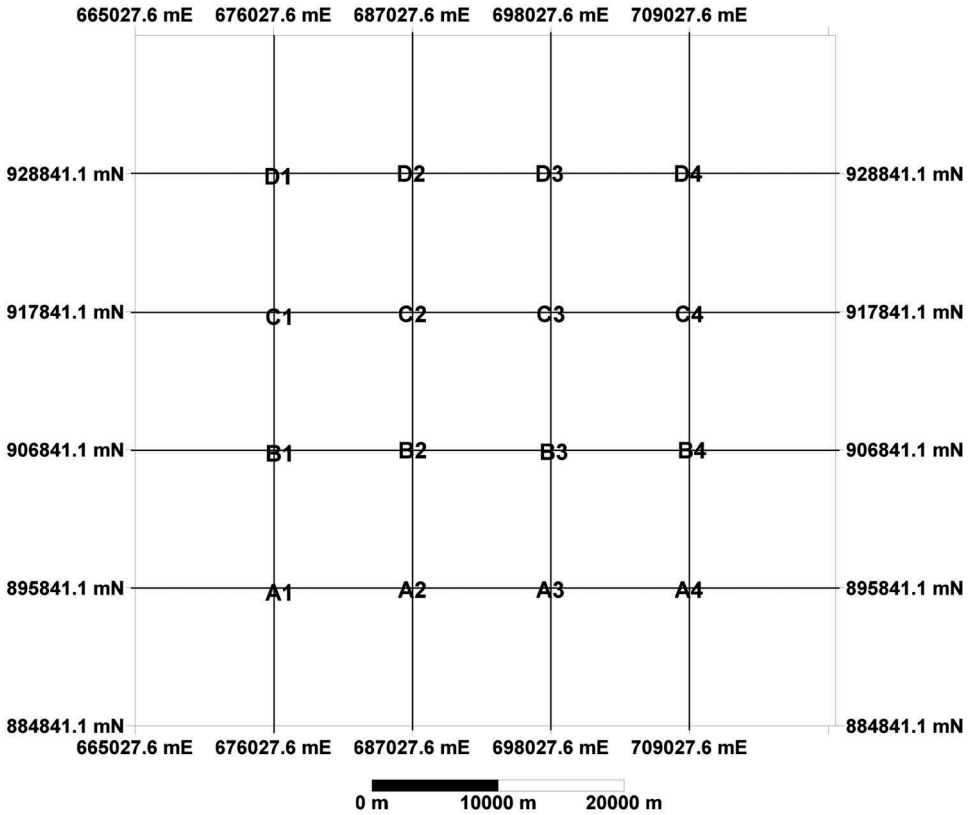


**Figure 8.** A layout of the study area. A1, A2 and D4 represent the centre of a 22,000 m × 22,000 m sub-grid.

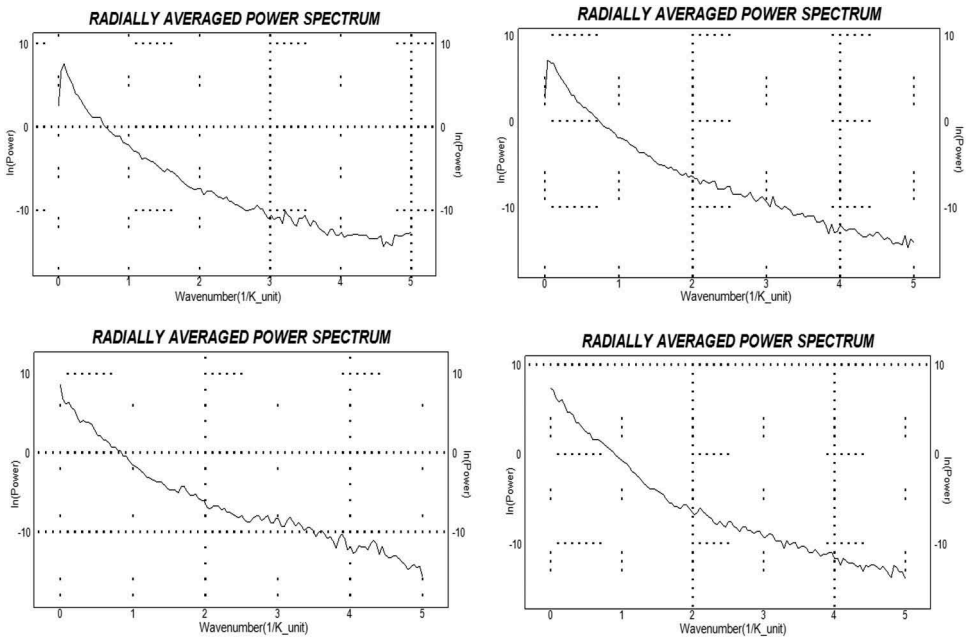


**Figure 9.** Radially averaged power spectrum of blocks A1 (top left), B2 (top right), C3 (bottom left) and D4 (bottom right).

### 5.6. The old and the new stress pattern in the near crust

The image of the depth to the top of the bedrock, better represented by the 3D image of the study area (Figure 10(b)), has revealed the displacement trends and the extent of displacement of the near surface crustal blocks, hence the stress pattern that has helped to shape the near crust (shallow parts of the continental crust) in the past. It was noted however that the planes of faults mapped from more recent geological field mapping efforts (Figures 3 and 10(a)) do not coincide nor lie along the bedrock margins (displacement margins) on the map of the depth to the top of the bedrock, but rather it cut through those margins. This indicates that these mapped faults are not genetically related with the formation of the bedrock

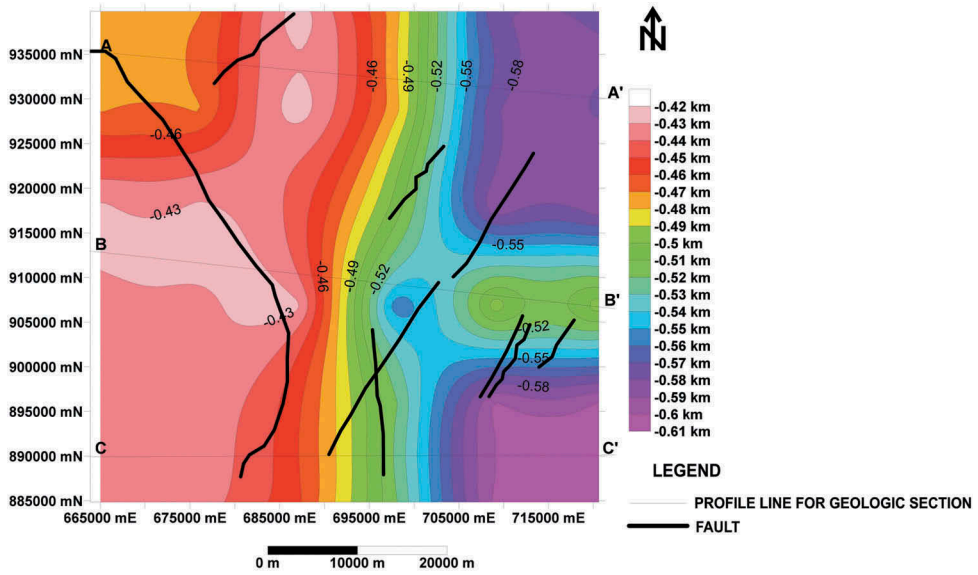


(a): Map of the Depth to the Top of Bedrock

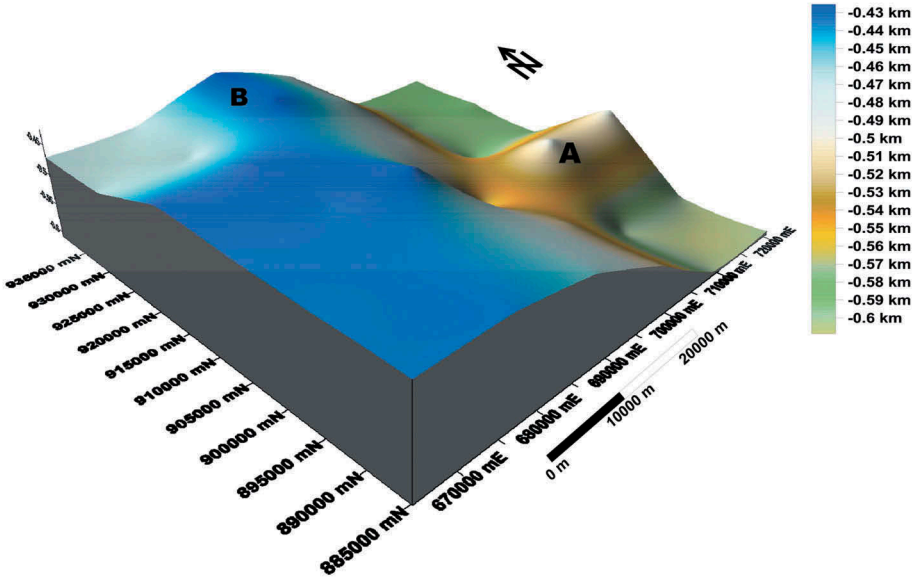


(b): 3D Image of the Depth to the Top of Bedrock

**Figure 10.** (a) Map of the depth to the top of bedrock. (b) 3D image of the depth to the top of bedrock.

margins (displacement margins) shown on Figure 10(a, b), but are rather new sets of faults reflecting the new stress pattern and condition at the near crust. This invariably means that the stress condition/pattern that defined the crustal deformation pattern at the near crust in the past has changed and is therefore different form the prevalent pattern that is dominant presently.

## 6. Conclusion

High-resolution aeromagnetic data acquired over Ilorin area (Nigeria), an area known for adjacent occurrence of extensive Migmatite–Gneiss–Quartzite complex and Schist Belt, were analysed and interpreted to gain more insight about the geologic settings and structural disposition of the area.

The notable anomalies observed on the residual magnetic field map were NE-SW trending magnetic anomalies (highs and lows) aligned diagonally and forming a distinct band with a width of between 16 and 20 km, coinciding with the Banded Gneiss region found in the central part of the study area; conspicuously discordant E-W trending magnetic low around the north-western region of the study area whose location was found to be around some portion of the boundary between Migmatite and Banded Gneiss when checked against the geologic map, and a ring-like magnetic low in the south-eastern region, having its centre at coordinates 699,039 m E and 892,747 m N, which is buried totally within the schist with no surface expression on the geologic map.

Two categories of linear features were outlined on the THD map. The first category was the relatively

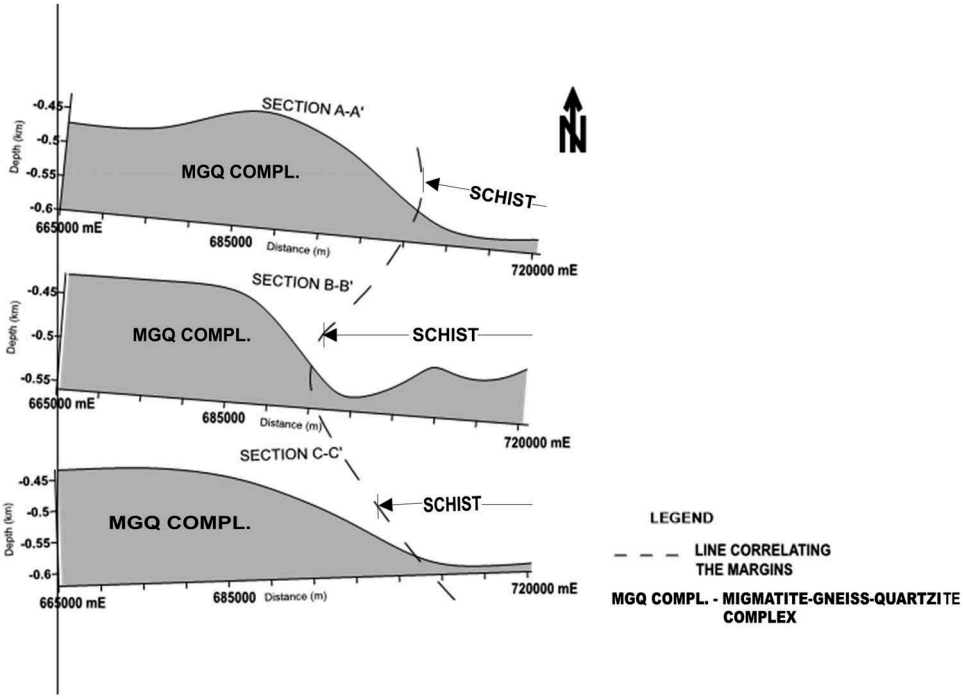


**Figure 11.** Stacked profile of profiles taken over Figure 10(a).

short, peak amplitudes concentrated within the region of the Banded Gneiss which indicated that the Banded Gneiss region is highly sheared and/or foliated. The second category was the relatively longer, continuous, lineaments which are of regional scale, trending mostly in the NE-SW direction and seeming to represent major lithologic boundaries.

The most extensive of these relatively longer lineaments are lineaments $M_1$ and $M_2$ which appeared more like lithological boundaries bounding the Banded Gneiss to the West and East respectively when the THD map was compared with the geologic map.

The concentration of many minor lineaments around $M_1$ and $M_2$ suggested that the lithological boundaries $M_1$ and $M_2$ themselves might be coincident with fracture zones such that the lithological boundaries were established over some major fractures (joints or faults) trending in the same manner as $M_1$ and $M_2$. If this were to hold true, then the major fractures supposedly coinciding with boundaries $M_1$ and $M_2$ were the possible channels from which heat was removed (leached) in the regional system during metamorphism such that the Banded Gneiss region (bounded by $M_1$ and $M_2$) attained a relatively lower grade metamorphism than the Migmatite adjacent to it.

From spectral analysis it was observed that at the western region of the study area, the depth to the magnetic basement ranged between 0.428 and 0.471 km while at the easternmost one-third region, the depth to the magnetic basement was found to be deeper, ranging between 0.477 and 0.602 km. The abruptness in the depth change as we move towards the easternmost region where schist is the principal lithology suggested that the magnetic basement in the easternmost region could have been downthrown relative to that in the western region. The maximum vertical displacement of the downthrown block of the easternmost region from the hanging block of the western region is about 174 m.

It was also noted that since the planes of faults mapped from more recent geological field mapping efforts do not coincide nor lie along the bedrock margins delineated from the map generated for the depth to the top of the magnetic basement but rather cut through those margins, the mapped faults were not genetically related with the formation of the bedrock margins but are rather new sets of faults reflecting the new stress pattern and condition at the near crust.

Though the ring-like anomaly labelled "Q" on the residual magnetic map would fall within the schist region if it were positioned on the geologic map, no unique surface structural or lithological expression was found to be corresponding to it on the geologic map. This could mean that the causative body is either intrusive or has not be mapped geologically. Coring and wireline logging is recommended at the centre of this anomaly if follow-up geologic field mapping confirmed that it is intrusive.

## Acknowledgements

The contribution of Mr Abimola Chris Ogunyele who made himself available for discussion on the geology of the study area is highly appreciated. I equally appreciate the efforts of Dr Akinola S. Akinwumiju and Mr Oluwaseyi E. Olajuyigbe who helped with the digital elevation model data.

## Disclosure statement

No potential conflict of interest was reported by the author.

## References


Ajibade AC, Woakes M, Rahaman MA. 1987. Proterozoic crustal development in the Pan-African regime of Nigeria. In: Kroner A, editor. Proterozoic lithospheric evolution. Washington DC (USA): American Geophysical Union; p. 259–271.

Balogun OB, Ojo SB, Olorunfemi MO. 2016. Characterization of tectonic lineaments in the central equatorial atlantic region of Africa from bouguer anomaly gravity data. Ife J Sci. 18(4):931–947.

Connard G, Couch R, Gemperle M. 1983. Analysis of Aeromagnetic measurement from the cascade range in central oregon. Geophysics. 48:376–390.

Dada SS. 1998. Crust-forming ages and proterozoic crustal evoluton in Nigeria: a reappraisal of current interpretations. Precambrian Res. 87:65–74.

Dada SS. 1999. Geochemistry and petrogenesis of the reworked archaean gneissic complex of northcentral Nigeria: major and trace element studies on kaduna amphibolites and migmatitic gneiss. Global J Pure Appl Sci. 5:535–543.

Hogg S. 2004. *GT-gradient tensor gridding, geologic structure example*. [accessed 2015 July]. http://www. shapegeophysics.com/.2004.

Naidu PS. 1972. Maximum likelihood (ML) estimation of depth from the spectrum of aeromagnetic fields. Geophysics. 95:141–149.

Ndougsa-Mbarga, T, Feumoe, AN, Manguelle-Dicoum E, and Fairhead JD 2012. Aeromagnetic data interpretation to locate buried faults in south-east cameroon. Geophysica. 48(1–2):49–63.

Oyeniyi TO, Salami AA, Ojo SB. 2016. Magnetic surveying as an aid to geological mapping: a case study from Obafemi Awolowo university campus in Ile-Ife, southwest Nigeria. Ife J Sci. 18(2):335.

Phillips JD. 2000. Locating magnetic contacts: A comparison of horizontal gradients, analytic signal and wave number methods. In 70th Annual International meeting, Calgary; SEG.

Phillips JD. 2002. Processing and interpretation of aeromagnetic data for the Santa Cruz basin – patahonia mountains area, south- central Arizona, in U.S. Geol Surv Open-File Rep. 2002–2098. [accessed 2019 May]. http://pubs.er.usgs.gov/publication/ofr0298

Reid AB, Allsop JM, Granser H, Millett AJ, Somerton IW. 1990. Magnetic interpretation in three dimensions using Euler deconvolution. Geophysics. 55:80–90.

Salem A, Williams S, Fairhead JD, Ravat D, Smith R. 2007. Tilt-depth method: a simple depth estimation method using first-order magnetic derivatives. Leading Edge. 26 (12):1502–1505.

Spector A, Grants FS. 1970. Statistical models for interpreting aeromagnetic data. Geophysics. 35:293–302.

Thompson DT. 1982. EULDPH: A new technique for making computer-assisted depth estimates from magnetic data. Geophysics. 47:31–37.

Turner DC. 1983. Upper proterozoic schist belts in the Nigerian sector of the Pan-African province of west Africa. Precambrian Res. 21(1–2):55–79.

USGS. 2006. Shuttle radar topography mission, 1 Arc second scene, filled-finished-B, global land cover facility. Maryland:University of Maryland, College Park.

Verduzco B, Fairhead JD, Green CM, MacKenzie C. 2004. New Insights into magnetic derivatives for structural mapping. Leading Edge. 23:116–119.

Woakes M, Rahaman MA, Ajibade AC. 1987. Some metallogenetic features of the Nigerian basement. J Afr Earth Sci. 6:54–64.